Available online at www.sciencedirect.com

ScienceDirect

Energy Procedia 4 (2011) 101–108

Energy Procedia

www.elsevier.com/locate/procedia

GHGT-10

Accurate screening of amines by the Wetted Wall Column

Xi Chen, Fred Closmann, Gary T. Rochelle*

Department of Chemical Engineering, The University of Texas at Austin, 1 University Station C0400, Austin, Texas 78712, USA

Abstract

To screen amine solvents accurately for CO_2 capture, a Wetted Wall Column (WWC) was used to measure equilibrium CO_2 partial pressure and CO_2 absorption/desorption rate at variable CO_2 loading from 40 to 100 °C. The solvents included 10 m diglycolamine (DGA®), 4.8 m 2-amino-2-methyl-propane (AMP), 8 m N-methyl-1,3-propanediamine (MAPA), 7 m/2 m and 5 m/5 m methyldiethanolamine (MDEA)/piperazine (PZ). With a semi-empirical VLE model assuming a lean/rich CO_2 loading corresponding to 500 Pa/5000 Pa CO_2 partial pressure, cyclic capacity and heat of CO_2 absorption was determined. Liquid film mass transfer coefficients are reported for each solvent, which allows estimation of packing area required for 90% removal via a simple absorber design. The results show that the capacity of DGA® and MAPA is 10–20% less than 7 m MEA with a 5 to 15% slower rate. 4.8 m AMP has a capacity twice as great as 7 m MEA, but the rate is lower by 45%. 7 m/2 m MDEA/PZ has a similar capacity to 8 m PZ but slightly slower rate. 5 m /5 m MDEA/PZ has a capacity 20% greater than 8 m PZ and a comparable rate. The heat of CO_2 absorption in the primary amines is about 80 kJ/mol CO_2. The value for PZ and its blend with MDEA is about 70 kJ/mol CO_2.

Keywords: Amine screening; Absorption/desorption rates; Cyclic capacity; Heat of CO_2 absorption.

1. Introduction

Amine solvents for CO_2 capture require high absorption/desorption rate, high capacity for CO_2, low degradation rate, and low volatility. A high heat of CO_2 absorption is also required to reduce overall energy consumption in amine regeneration and CO_2 compression [1, 2]. Efforts in amine screening have been reported by many researchers [3-8]. Most of them measure relative absorption/desorption rate by simple CO_2 sparging, which lacks the ability to estimate amine performance in a real absorber. Furthermore, cyclic capacity and heat of absorption at practical conditions are rarely available in these studies.

A wetted wall column (WWC) has been extensively utilized to study kinetics between amines and CO_2. However, few of these studies use practical levels of CO_2 loading and amine concentration [9-13]. Because it closely approximates mass transfer between gas and liquid on real packing, a WWC provides an excellent platform to evaluate new amine solvents.

In this study, CO_2 solubility and the absorption/desorption rate in five amine solvents, 10 m DGA®, 4.8 m AMP, 8 m MAPA, 7 m/2 m and 5 m/5 m MDEA/PZ were measured in a WWC at 40 °C to 100 °C with variable CO_2

* Corresponding author. Tel.: +1-512-471-7230; fax: +1-512-475-7824.
E-mail address: gtr@che.utexas.edu.

doi:10.1016/j.egypro.2011.01.029

loading. The CO_2 loading (α, mol/mol alkalinity) was chosen to give a CO_2 partial pressure at 40 °C of 500 Pa to 5000 Pa to cover the expected range for post-combustion capture from a coal-fired power plant. Equilibrium CO_2 partial pressure (P_{CO2}^*) and liquid film mass transfer coefficient (k_g') were measured at each condition. The obtained solubility data was modelled with a semi-empirical correlation, which enables calculation of cyclic capacity and heat of CO_2 absorption.

2. Experimental methods and materials

A schematic of the entire WWC apparatus is shown in Figure 1. Details of the WWC are shown in Figure 2. This is the same apparatus and method as used by Bishnoi [14], Cullinane [12], Dugas [13], and Chen et al. [15].

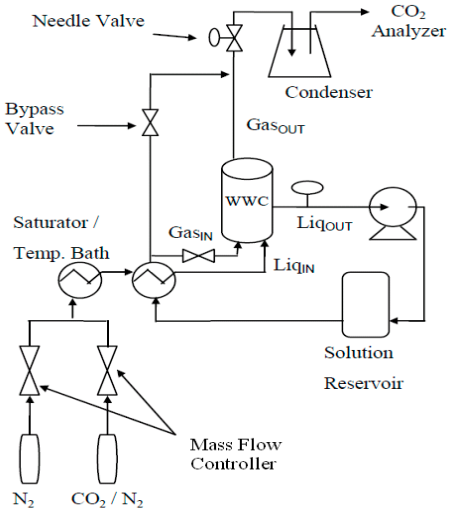

Figure 1. Flow sheet of the WWC apparatus.

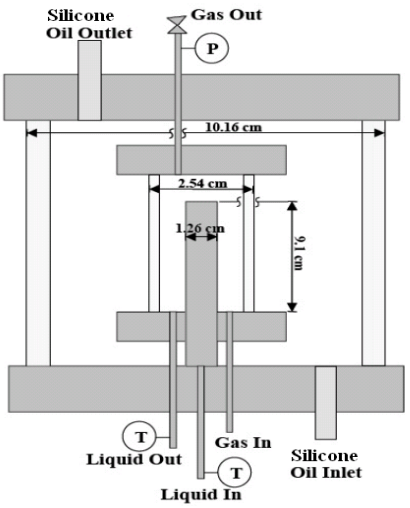

Figure 2. Detailed view of the WWC.

A CO_2/N_2 mixture was fed into the WWC by mass flow controllers at 5×10^{-3} standard m^3/min. The inlet partial pressure of CO_2 was varied from zero to about double the equilibrium pressure. The gas mixture was saturated with water and further heated by an oil bath before entering the WWC chamber from the bottom. Liquid in a one-liter reservoir was pumped through the middle of the column and overflowed from the top. Then it evenly distributed along the outer surface of the column and exited the bottom, counter-currently contacting the gas. The liquid was recirculated at 2.4×10^{-4} m^3/min. The total pressure of the system was regulated between 0.2 MPa to 0.7 MPa with a needle valve at the gas outlet. The gas exiting from the top was directed through a condenser and a desiccation unit to remove water and amine vapor. The outlet CO_2 concentration was measured continuously by an infrared CO_2 analyzer (Horiba 2000). The bypass valve allows direct measurement of inlet CO_2 concentration.

Typically six inlet CO_2 partial pressures were selected for each CO_2 loading and temperature (T), as shown in Figure 3. Three of them are greater than the equilibrium CO_2 partial pressure of the solution, leading to absorption of CO_2 and positive flux; while the other three correspond to desorption. CO_2 flux and driving forces between gas and liquid, which are determined from the difference of inlet and outlet CO_2 concentration, can be correlated by a line. The slope of the line represents the overall mass transfer coefficient (K_G):

$$K_G = \frac{N_{CO_2}}{P_{CO_2,g} - P^*_{CO_2}} \tag{1}$$

where N_{CO2} is CO_2 flux and $P_{CO2,g}$ is CO_2 partial pressure in the bulk gas.

The line is shifted along the abscissa axis by adjusting P_{CO2}^* until it almost crosses the original point, where the driving force is zero and no flux should be observed. In this way, P_{CO2}^* is determined as a function of loading and temperature.

A pre-determined correlation for gas film mass transfer coefficient (k_g) [14] is combined with the experimental results for K_G to calculate liquid film mass transfer coefficient (k_g'):

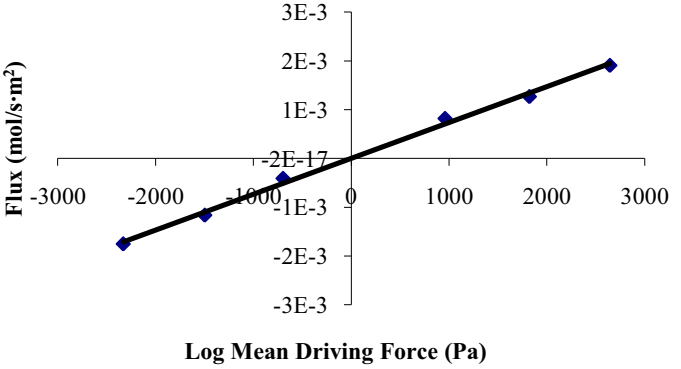

Figure 3. Flux as a function of log mean driving force between gas and liquid for 10 m DGA® at 60 °C and CO_2 loading of 0.4 mol/mol alkalinity.

$$\frac{1}{k_g^{'}} = \frac{1}{K_G} - \frac{1}{k_g} \tag{2}$$

k_g' is the CO_2 flux normalized by CO_2 partial pressure driving force between gas-liquid interface and bulk liquid. It is dependent on reaction kinetics, CO_2 solubility and diffusivity of reactants and products. Therefore k_g' is an inherent property of the amine solvent. If amine concentration can be assumed to be constant across the reaction boundary, the following approximation is valid:

$$k_g^{'} \approx \frac{\sqrt{D_{CO_2} k_2 [Am]_b}}{H_{CO_2}} \tag{3}$$

D_{CO2}, diffusivity of CO_2 in amine solution; k_2, second-order reaction rate constant; $[Am]_b$, free amine concentration in bulk solution; H_{CO2}, Henry's constant of CO_2 in amine solution.

DGA® (98%, Acros), AMP (99%, Acros), MAPA (99%, Alfa Aesar), MDEA (99%, Huntsman), PZ (anhydrous, 99%, Alfa Aesar) were used without purification for preparation of aqueous solution. CO_2 loading was determined by total inorganic carbon analysis [16]. Amine concentration was confirmed by amine titration [16].

3. Results and Discussion

3.1 CO_2 solubility

CO_2 solubility data in DGA® and AMP show good agreement with literature data (Figure 4 and Figure 5). A semi-empirical model (Equation 4), which assumes P_{CO2}^* (Pa) is only a function of CO_2 loading (α) and T (K), was used to fit the solubility data for each amine. Parameters for different amines are given in Table 1. With this model, lean and rich CO_2 loading corresponding to 500 and 5000 Pa at 40 °C were determined. The difference between lean and rich loading gives cyclic capacity of CO_2 for each amine.

$$\ln P_{CO_2}^* = a + b/T + c\alpha + d\alpha/T + e\alpha^2 \tag{4}$$

The heat of CO_2 absorption (ΔH_{abs}) is obtained using the Gibbs-Helmholtz equation:

$$\Delta H_{abs} = -R\frac{d(\ln P_{CO_2}^*)}{d(1/T)} = -R\cdot(b + d\cdot\alpha) \tag{5}$$

ΔH_{abs} is only dependent on CO_2 loading under the current model. ΔH_{abs} at the CO_2 loading corresponding to P_{CO2}^* = 1500 Pa is reported as an average value.

CO_2 solubility data for MAPA and MDEA/PZ are shown in Figure 6. In MAPA, free amine is depleted as CO_2 loading approaches 0.5 and P_{CO2}^* increases rapidly with loading. Therefore the CO_2 capacity of MAPA from 500 Pa to 5000 Pa is relatively small. In Figure 7, the solubility data for MDEA/PZ are compared to those from Bishnoi et al. [17] and Derks et al. [18] for 7.8 m MDEA/1.2 m PZ. Increases in the PZ fraction increase CO_2 solubility because PZ carbamate is a more stable form of CO_2.

Table 1. Regressed value of parameters for solubility model used in this work

Amine	a	b	c	d	e
7 m MEA	36.61±2.80	-11152±896	-7.46±8.36	2389±2636	26.69±2.58
8 m PZ	34.52±2.09	-10676±683	-10.10±7.27	7596±2370	14.43±3.27
10 m DGA®	53.57±5.61	-16434±2081	-48.85±15.13	14762±5798	34.28±11.18
8 m MAPA	53.45±9.84	-14517±3234	-78.86±25.91	9035±8009	103.75±17.99
4.8 m AMP	35.47±0.87	-10080±299	1.70±2.80	3258±966	-4.89±1.11
7m/2m MDEA/PZ	33.94±0.76	-9694±277	2.30±4.98	8054±1918	-29.46±3.88
5m/5m MDEA/PZ	34.68±1.76	-10792±602	6.98±7.97	8746±2612	-31.49±6.39

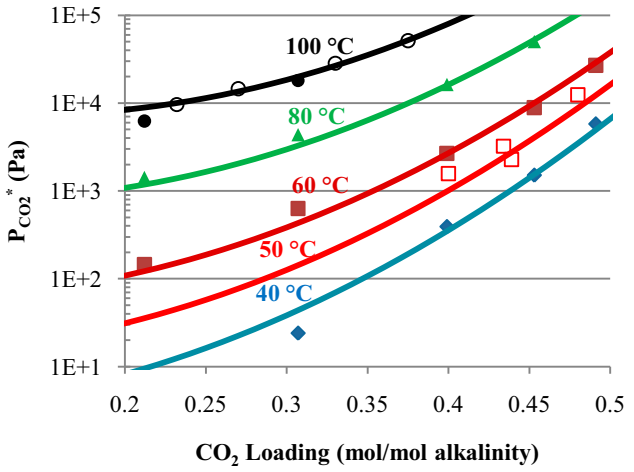

Figure 4. CO_2 solubility in 10 m DGA®. Filled points: experimental data; Solid lines: model prediction (Eq. 4); Open points: 14.3 m DGA® at 50 °C (square) and 100 °C (circle) from Ref. [19].

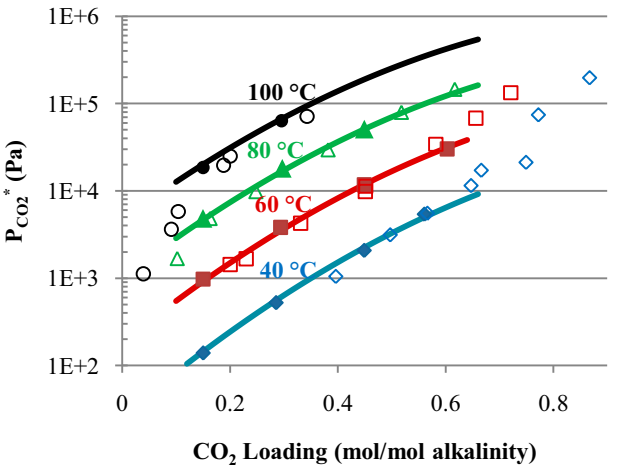

Figure 5. CO_2 solubility in 4.8 m AMP. Filled points: experimental data; Solid lines: model prediction (Eq. 4); Open points: Ref. [20].

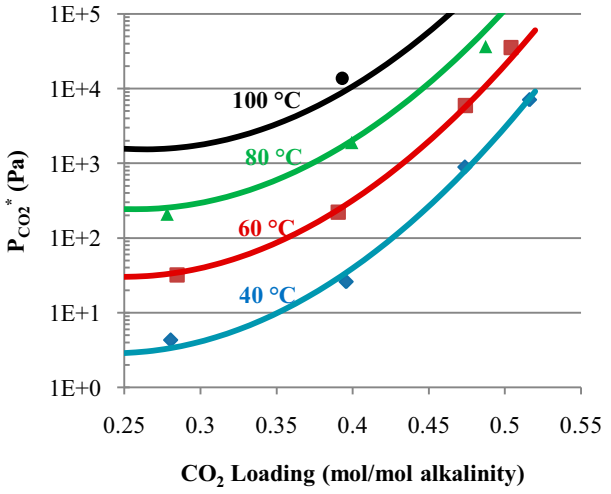

Figure 6. CO_2 solubility in 8 m MAPA. Filled points: experimental data; Solid lines: model prediction.

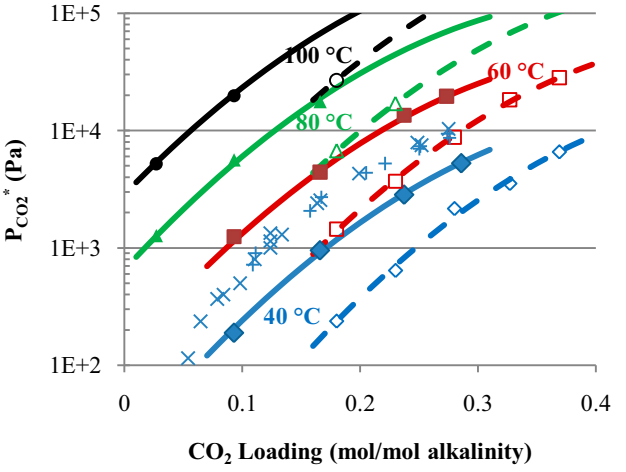

Figure 7. CO_2 solubility in MDEA/PZ. Filled points: experimental 7 m/2 m; Solid lines: model 7/2; Open points: experimental 5 m/5 m; Dashed lines: model 5/5; 7.8 m /1.2 m PZ at 40 °C by Bishnoi et al. [17] (×) and Derks et al. [18] (+).

3.2 Absorption/desorption rate

The rate data for the amines are shown in Figure 8 to Figure 11. k_g' values are shown as a function of P_{CO2}^* at 40 °C, a surrogate for loading. In general, an increase in T leads to equal or smaller k_g', with exceptions seen in AMP. This can be explained by Equation 3. Although D_{CO2} and k_2 both increase with T, H_{CO2} increases simultaneously. The change in k_g' depends on how these factors offset each other. Using the P_{CO2}^* instead of CO_2 loading as the x-axis also allows direct comparison of rates on the same basis for different amines. Data for 8 m PZ and 7 m MEA at 40 °C by Dugas et al. [13] are shown for comparison. As can be seen, CO_2 absorption in PZ is about 1.5 to 2 times faster than MEA. DGA® has a comparable rate to MEA from 20 Pa to 1000 Pa, presumably because that they are both unhindered primary amines. Although the reaction kinetics of AMP with CO_2 is approximately 10 times slower than MEA [21, 22] due to the steric hindered amino group, CO_2 absorption rate of AMP is found to be as high as half of MEA. A stoichiometric ratio of 1 mol CO_2/mol AMP results in higher free amine concentration, which compensates for small k_2. MAPA is a faster solvent than MEA at lean CO_2 partial pressure but much slower at the rich end.

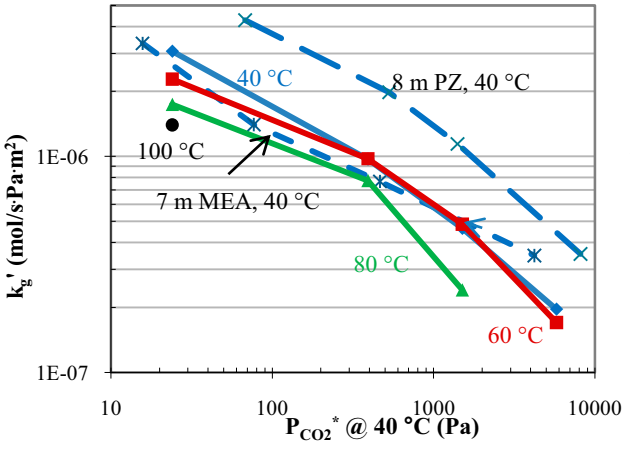

Figure 8. Liquid mass transfer coefficient (k_g') of 10 m DGA® (solid lines). The data is compared with k_g' for 7 m MEA (short dashed line) and 8 m PZ at 40 °C (long dashed line) [13].

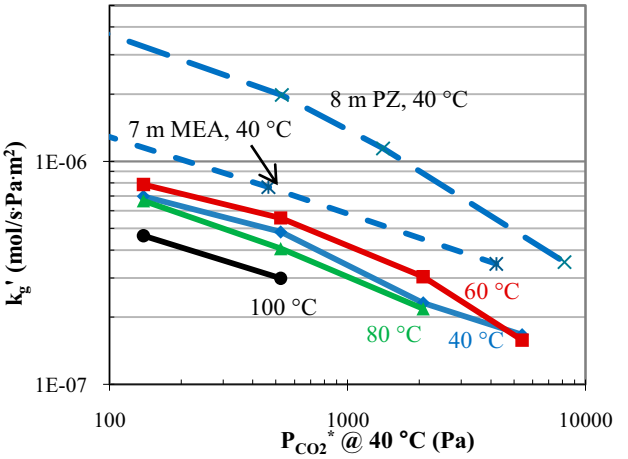

Figure 9. k_g' of 4.8 m AMP (solid lines).

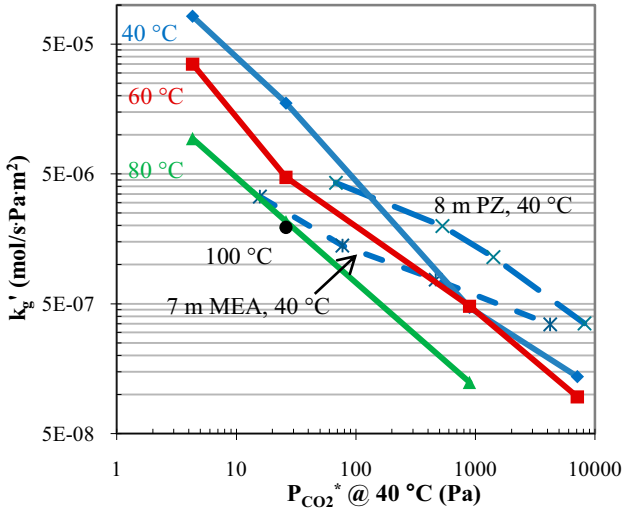

Figure 10. k_g' of 8 m MAPA (solid lines).

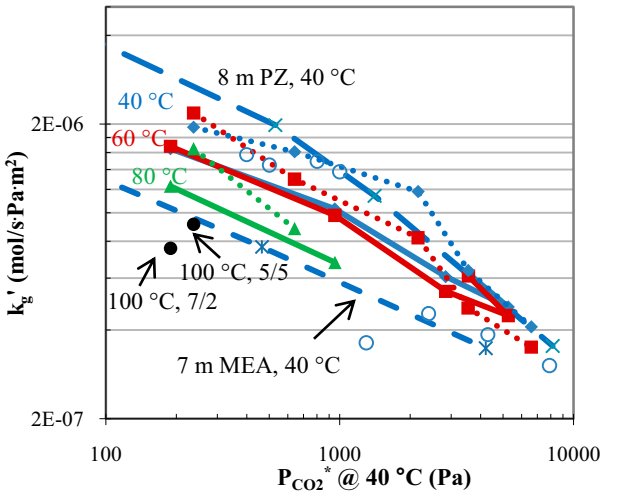

Figure 11. k_g' of 7 m/2 m (solid lines) and 5 m/5 m MDEA/PZ (dotted lines). Open circles: 7.8 m /1.2 m MDEA/PZ at 40 °C [17].

7 m/2 m MDEA/PZ is slightly slower than 8 m PZ at lean loading but similar at rich loading. This means PZ can greatly enhance CO_2 absorption rate even at a lower fraction. 5 m/5 m MDEA/PZ has a faster rate than 7/2 at all the temperatures. It also has a similar performance to PZ at 40 °C. kg' reported by Bishnoi et al. for 7.8 m/1.2 m MDEA/PZ [17] is greater than that for 7/2 and slightly less than 5/5 at lean loading, but slower than either 7/2 or 5/5 at rich end. In the blend, MDEA catalyzes the formation of PZ carbamate and becomes protonated, therefore there is still abundant free PZ available to react with CO_2, retaining higher absorption rate. All the solubility and rate data are given in Table 2.

Table 2. Equilibrium CO_2 partial pressure (P_{CO2}^*, kPa) and liquid film mass transfer coefficient (k_g', 10^{-7} mol/(s·Pa·m^2)) at varied CO_2 loading (α, mol/mol alkalinity) and temperature (T, °C)

T	α	P_{CO2}	k_g'
10 m DGA®			
40	0.307	0.02	30.7
	0.399	0.39	9.7
	0.453	1.51	4.6
	0.491	5.79	2.0
60	0.212	0.15	37.1
	0.307	0.63	22.8
	0.399	2.67	9.8
	0.453	8.87	4.9
	0.491	26.9	1.7
80	0.212	1.42	31.4
	0.307	4.36	17.4
	0.399	16.3	7.7
	0.453	50.1	2.4
100	0.212	6.25	24.5
	0.307	18.0	14.0

T	α	P_{CO2}	k_g'
4.8 m AMP			
40	0.15	0.14	7.0
	0.28	0.52	4.8
	0.44	2.08	2.3
	0.56	5.41	1.7
60	0.15	0.98	7.9
	0.29	3.81	5.6
	0.44	11.7	3.0
	0.60	30.2	1.6
80	0.15	4.85	6.7
	0.29	18.2	4.1
	0.44	51.0	2.2
100	0.15	18.5	4.6
	0.29	63.6	3.0

T	α	P_{CO2}	k_g'
8 m MAPA			
40	0.280	0.00	817.
	0.396	0.03	175.
	0.474	0.89	4.7
	0.516	7.12	1.4
60	0.285	0.03	350.
	0.390	0.22	47.0
	0.474	5.92	4.8
	0.504	35.3	1.0
80	0.278	0.21	93.5
	0.399	1.89	21.4
	0.487	36.4	1.2
100	0.393	13.8	19.4

T	α	P_{CO2}	k_g'
7 m MDEA/2 m PZ			
40	0.093	0.19	16.5
	0.166	0.95	10.3
	0.237	2.84	6.1
	0.286	5.26	4.8
60	0.093	1.25	16.8
	0.166	4.41	9.8
	0.237	13.5	5.4
	0.273	19.6	4.5
80	0.027	1.27	27.6
	0.093	5.62	12.3
	0.166	17.6	6.8
10	0.027	5.21	16.3
0	0.093	19.8	7.6
5 m MDEA/5 m PZ			
40	0.18	0.24	19.5
	0.23	0.64	16.1
	0.28	2.16	11.8
	0.33	3.54	6.4
	0.37	6.59	4.1
60	0.18	1.45	21.8
	0.23	3.70	13.0
	0.28	8.77	8.2
	0.33	18.3	4.8
	0.37	28.2	3.5
80	0.18	6.73	16.5
	0.23	16.9	8.8
10	0.18	26.7	9.1

3.3 Cyclic capacity and heat of CO_2 absorption

The calculated values for lean/rich CO_2 loading, capacity, and heat of absorption are given in Table 3. The capacity of 7 m/2 m MDEA/PZ is same as 8 m PZ, while that of the 5/5 blend is about 25% higher than 8 m PZ. If the total amount of alkalinity in each solvent is taken into account, it can be seen that the addition of MDEA to PZ effectively increases the CO_2 capacity while maintaining the fast kinetics associated with PZ. Tertiary amines like MDEA cannot form carbamate with CO_2. Instead, 1 mol MDEA reacts with 1 mol CO_2 to produce bicarbonate and protonated MDEA. 4.8 m AMP has a CO_2 capacity two times as great as that of MEA and about 20% higher than PZ, even at a lower amine concentration. This is attributed to the hindered nature of AMP. However the CO_2 capacity of 10 m DGA® and 8 m MAPA are only about half of 8 m PZ and slightly smaller than 7 m MEA.

The heat of CO_2 absorption for PZ and its blend with MDEA is about 70 kJ/mol CO_2. ΔH_{abs} for AMP is slightly higher than PZ. All of the primary amines, MEA, DGA® and MAPA, have a value slightly greater than 80 kJ/mol CO_2, presumably because of the greater heat of reaction in carbamate formation.

3.4 Application of rate data

Accurate measurement of absorption rates makes it possible to accomplish simple absorber design. k_g' values at P_{CO2}^* = 500 Pa and 5000 Pa at 40 °C for each amine are interpolated/extrapolated from available data. These two values represent the rate of mass transfer at the top and bottom of an isothermal absorber operated at 40 °C. The CO_2 flux is then equal to k_g' times the driving force. An average value of k_g' is generated by dividing the log mean flux by the log mean driving force at the top and bottom (Equation 6):

$$k'_{g,avg} = \frac{Flux_{CO_2,LM}}{(P_{co_2,gas} - P^*_{co_2})_{LM}} = \frac{(Flux_{CO_2,top} - Flux_{CO_2,bottom}) / \ln(Flux_{CO_2,top} / Flux_{CO_2,bottom})}{[(P_{co_2,top} - P^*_{co_2,lean}) - (P_{co_2,bottom} - P^*_{co_2,rich})] / \ln(\frac{P_{co_2,top} - P^*_{co_2,lean}}{P_{co_2,bottom} - P^*_{co_2,rich}})} \quad (6)$$

This value reflects the average absorption rate over the whole absorber column. The packing area (A_p) required for unit volumetric flow rate of flue gas (V_g) can also be estimated with the assumption of 90 % CO_2 removal.

$$A_p / V_g = \frac{90\% \times 12\% \times P / RT}{Flux_{CO_2,LM}} \quad (7)$$

The average value of k_g' as well as A_p/V_g are shown in Table 3. 8 m PZ has the fastest CO_2 mass transfer rate, corresponding to the least packing area requirement, 1800 $m^2/(m^3/s)$. 7 m MEA is only 50% as fast as PZ, which doubles the required packing area. 5 m /5 m MDEA/PZ has a similar rate to PZ, while 7/2 is roughly 15% slower. CO_2 absorption in 10 m DGA® and 8 m MAPA are slower than in MEA by 5–15%. 4.8 m AMP, as the slowest solvent, requires a packing area up to 6300 $m^2/(m^3/s)$.

Table 3. Overview of properties for all the amines tested. PZ and MEA [13] and N-methyl PZ and 2-methyl PZ data [15] are also included.

Amine	Lean/Rich loading (mol CO_2/mol alkalinity)	Cyclic CO_2 Capacity (mol/kg (water+amine))	$-\Delta H_{abs}$ @P_{CO2} =1.5kPa (kJ/mol)	$k_g'_{avg}$@40°C ($\times 10^7$mol/s·Pa·m^2)	A_p/V_{fg} (10^3 m^2/(m^3/s))
8 m PZ	0.31/0.39	0.79	70	8.5	1.8
8 m N-methyl PZ	0.16/0.26	0.83	67	8.4	1.8
5m/5m MDEA/PZ	0.21/0.35	0.99	70	8.3	1.8
7m/2m MDEA/PZ	0.13/0.28	0.80	68	6.9	2.2
8 m 2-methyl PZ	0.27/0.37	0.93	72	5.9	2.6
7 m MEA	0.45/0.55	0.47	82	4.3	3.5
10 m DGA®	0.41/0.49	0.38	81	3.6	4.2
8 m MAPA	0.47/0.51	0.42	84	3.1	4.8
4.8 m AMP	0.27/0.56	0.96	73	2.4	6.3

4. Conclusions

The measurements of CO_2 solubility and absorption/desorption rates with the Wetted Wall Column enable the extraction and comparison of CO_2 capacity, heat of absorption, and mass transfer rates in different amine solvents. The primary amines studied, DGA® and MAPA, along with MEA, suffer from low CO_2 capacity and absorption rates. However, their high heat of absorption would help lower the energy requirement and could offset their disadvantages. 4.8 m AMP has a high CO_2 capacity, but its application as a CO_2 capture solvent could be hindered by its low CO_2 absorption rate. MDEA blended with PZ shows great promise with its high CO_2 capacity and absorption rate, if compromised with the relatively lower heat of absorption.

The packing area for unit volume of flue gas is estimated in a simple absorber design. Fast amines such as 5 m /5 m MDEA/PZ, only require 1/2 to 1/3 of the packing area that would be needed for slow solvents like DGA®, MAPA, and AMP. Therefore a fast amine would greatly reduce the column size and capital cost.

5. Acknowledgement

The authors acknowledge the support of the Luminant Carbon Management Program.

6. References

[1] Oyenekan BA, Rochelle GT. Energy Performance of Stripper Configurations for CO_2 Capture by Aqueous Amines. Ind. Eng. Chem. Res. 2006; 45(8): 2457-2464.
[2] Oexmann J, Kather A. Minimising the regeneration heat duty of post-combustion CO_2 capture by wet chemical absorption: The misguided focus on low heat of absorption solvents. 2009; 4(1): 36-43.
[3] Hook RJ. An Investigation of Some Sterically Hindered Amines as Potential Carbon Dioxide Scrubbing Compounds. Ind. Eng. Chem. Res. 1997; 36(5): 1779-1790.
[4] Mimura T, et al. Evaluation of alkanolamine chemical absorbents for CO_2 from vapor-liquid equilibrium measurements. Kagaku Kogaku Ronbunshu 2005; 31(4): 237-242.
[5] Singh P, Niederer JPM, Versteeg GF. Structure and activity relationships for amine based CO_2 absorbents-I. Int. J. Greenhouse Gas Control 2007; 1(1): 5-10.
[6] Singh P, Versteeg GF. Structure and activity relationships for CO_2 regeneration from aqueous amine-based absorbents. Process Saf. Environ. Prot. 2008; 86(5): 347-359.
[7] Singh P, Niederer JPM, Versteeg GF. Structure and activity relationships for amine-based CO_2 absorbents-II. Chem. Eng. Res. Des. 2009; 87(2): 135-144.
[8] Puxty G, et al. Carbon Dioxide Postcombustion Capture: A Novel Screening Study of the Carbon Dioxide Absorption Performance of 76 Amines. Environ. Sci. Technol. 2009; 43(16): 6427-6433.
[9] Al-Juaied M, Rochelle GT. Absorption of CO_2 in aqueous blends of diglycolamine and morpholine. Chem. Eng. Sci. 2006; 61(12): 3830-3837.
[10] Pacheco MA, Kaganoi S, Rochelle GT. CO_2 absorption into aqueous mixtures of diglycolamine and methyldiethanolamine. Chem. Eng. Sci. 2000; 55(21): 5125-5140.
[11] Bishnoi S, Rochelle GT. Absorption of carbon dioxide in aqueous piperazine/methyldiethanolamine. AIChE J. 2002; 48(12): 2788-2799.
[12] Cullinane JT, Rochelle GT. Carbon dioxide absorption with aqueous potassium carbonate promoted by piperazine. Chem. Eng. Sci. 2004; 59(17): 3619-3630.
[13] Dugas R, Rochelle G. Absorption and desorption rates of carbon dioxide with monoethanolamine and piperazine. Energy Procedia 2009; 1(1): 1163-1169.
[14] Bishnoi S, Rochelle GT. Absorption of carbon dioxide into aqueous piperazine: reaction kinetics, mass transfer and solubility. Chem. Eng. Sci. 2000; 55(22): 5531-5543.
[15] Chen X, Rochelle GT. Aqueous Piperazine Derivatives for CO_2 Capture: Accurate Screening by a Wetted Wall Column. Submitted to Chem. Eng. Res & Des. 2010.
[16] Freeman SA, et al. Carbon dioxide capture with concentrated, aqueous piperazine. Energy Procedia 2009; 1(1): 1489-1496.
[17] Bishnoi S. Carbon dioxide absorption and solution equilibrium in piperazine activated methyldiethanolamine Department of Chemical Engineering 2000; Ph.D. Dissertation.
[18] Derks PWJ, Hogendoorn JA, Versteeg GF. Experimental and theoretical study of the solubility of carbon dioxide in aqueous blends of piperazine and N-methyldiethanolamine. J. Chem. Thermodyn. 2009; 42(1): 151-163.
[19] Martin JL, Otto FD, Mather AE. Solubility of hydrogen sulfide and carbon dioxide in a diglycolamine solution. J. Chem. Eng. Data 1978; 23(2): 163-4.
[20] Li M-H, Chang B-C. Solubilities of Carbon Dioxide in Water + Monoethanolamine + 2-Amino-2-methyl-1-propanol. J. Chem. Eng. Data 1994; 39(3): 448-52.
[21] Alper E. Reaction mechanism and kinetics of aqueous solutions of 2-amino-2-methyl-1-propanol and carbon dioxide. Ind. Eng. Chem. Res. 1990; 29(8): 1725-8.
[22] Saha AK, Bandyopadhyay SS. Kinetics of absorption of CO_2 into aqueous solutions of 2-amino-s-methyl-1-propanol. Chem. Eng. Sci. 1995; 50(22): 3587-98.